Influence of Head Tissue Conductivity in Forward and Inverse Magnetoencephalographic Simulations Using Realistic Head Models

Robert Van Uitert*, *Student Member, IEEE*, Chris Johnson, *Senior Member, IEEE*, and Leonid Zhukov

***Abstract*—The influence of head tissue conductivity on magnetoencephalography (MEG) was investigated by comparing the normal component of the magnetic field calculated at 61 detectors and the localization accuracy of realistic head finite element method (FEM) models using dipolar sources and containing altered scalp, skull, cerebrospinal fluid, gray, and white matter conductivities to the results obtained using a FEM realistic head model with the same dipolar sources but containing published baseline conductivity values. In the models containing altered conductivity values, the tissue conductivity values were varied, one at a time, between 10% and 200% of their baseline values, and then varied simultaneously. Although changes in conductivity values for a single tissue layer often altered the calculated magnetic field and source localization accuracy only slightly, varying multiple conductivity layers simultaneously caused significant discrepancies in calculated results. The conductivity of scalp, and to a lesser extent that of white and gray matter, appears especially influential in determining the magnetic field. Comparing the results obtained from models containing the baseline conductivity values to the results obtained using other published conductivity values suggests that inaccuracies can occur depending upon which tissue conductivity values are employed. We show the importance of accurate head tissue conductivities for MEG source localization in human brain, especially for deep dipole sources or when an accuracy greater than 1.4 cm is needed.**

***Index Terms*—Finite element method, MEG, source localization, tissue conductivity.**

I. Introduction

MAGNETOENCEPHALOGRAPHY (MEG) measures the extracranial magnetic fields produced by neuronal activity within the brain. A standard method for modeling the macroscopic neural activity assumes that such activity can be represented by electric current dipoles. The electric currents produced by the dipoles contain two components: the primary current, which represents the source of neural activity, and the secondary or volume current, which results from the interaction of the primary current with a conductive medium [1], [2]. MEG detectors measure the normal component of the net magnetic field due to both primary and secondary currents.

Simulations that calculate the magnetic fields resulting from current dipoles, the forward problem, most commonly use models consisting of a set of concentric spheres, each with homogeneous and isotropic conductivity [3], [4]. Such spherical models reduce the MEG forward problem to a closed form analytic solution, which is independent of the conductivities of the different head tissue layers [5]. The spherical model, however, may be less accurate than the realistic head model [6] in representing the human head for MEG, although more realistic, inhomogeneous, nonspherical head models are burdened by the fact that in these models a closed form solution cannot be computed and approximation methods, such as finite or boundary element methods, must be used.

Spherical models can ignore volume currents, but in realistic head models, volume currents are important in determining magnetic fields [7], and tissue conductivity values must be considered in the calculations of volume currents. Unfortunately, the conductivity values of tissues used in realistic head models vary greatly in the literature. The scalp conductivity values have been reported to be between 0.33 S/m–1.0 S/m, skull conductivity values vary between 0.0042 S/m–0.05 S/m, cerebrospinal fluid (CSF) conductivity values range between 0.33 S/m–3.00 S/m, and gray and white matter conductivity values are reported to be between 0.33 S/m–1.0 S/m and 0.31 S/m–0.48 S/m, respectively [8]–[15]. We used the finite element method (FEM) [16]–[18] to investigate the effects that various head tissue conductivities have on the total magnetic field produced by a dipolar source and measured at MEG detectors, and their importance in accurately calculating the normal component of the magnetic field detected by MEG.

The MEG inverse problem determines a current dipole's location within the head from the normal component of the magnetic field located at each detector, and relies on the techniques and modeling of the forward problem. After determining the influence of various head tissue conductivities in the forward simulations, we performed inverse simulations on the realistic head models to investigate the affect of altering tissue conductivities on accurate dipole source localization.

II. Background

The distribution of electric and magnetic fields in and surrounding the head can be found from Maxwell's equations. Considering the head as containing conductive regions G_i with con-

Manuscript received November 19, 2003; revised May 2, 2004. This work was supported in part by the National Institutes of Health (NIH) under NCRR Grant 5P41RR012553-02. *Asterisk indicates corresponding author.*

*R. Van Uitert is with the Scientific Computing and Imaging Institute, University of Utah, 50 South Central Campus Drive, Room 3490, Salt Lake City, UT 84112 USA (e-mail: vanuiter@cs.utah.edu).

C. Johnson is with the Scientific Computing and Imaging Institute, University of Utah, Salt Lake City, UT 84112 USA.

L. Zhukov is with the Department of Computer Science, California Institute of Technology, Pasadena, CA 91125 USA.

Digital Object Identifier 10.1109/TBME.2004.836490

0018-9294/04$20.00 © 2004 IEEE

ductivities σ_i and having constant magnetic permeability equivalent to that of free space, $\mu_i = \mu_0$, the quasi-static approximation of Maxwell's equations is given by

$$\nabla \times \vec{E} = 0; \quad \nabla \cdot \vec{E} = 0 \tag{1}$$

$$\nabla \times \vec{B} = \mu_0 \vec{J}; \quad \nabla \cdot \vec{B} = 0. \tag{2}$$

The electromotive force impressed by biological activity on conducting tissues produces the dipole's primary current density, $\vec{J}_p$ [5]. The returning, passive current, within the conductor can be computed using Ohm's law $\vec{J}_r = \sigma \vec{E}$. Then the total current within a conductor is given by

$$\vec{J} = \vec{J}_p + \sigma \vec{E}. \tag{3}$$

The curl free electric field can be represented through the gradient of its potential $\vec{E} = -\nabla\phi$ and (3) becomes

$$\vec{J} = \vec{J}_p - \sigma \nabla \phi. \tag{4}$$

Finally, the continuity equation for a closed system can be written as

$$\nabla \cdot \vec{J} = 0. \tag{5}$$

Combining (4) with (5), we derive the Poisson equation, which describes the distribution of potential and, therefore, electric fields and currents inside the conductor

$$\nabla \cdot (\sigma \nabla \phi) = \nabla \cdot \vec{J}_p. \tag{6}$$

That the solution of the Poisson equation should satisfy Neumann boundary conditions on the surface of the head, $\partial\phi/\partial n = 0$, also follows from Maxwell's equations.

The permeability of the head is indistinguishable from that of the surrounding volume and, thus, there are no boundary conditions on the surface of the head to be satisfied for the magnetic field. Magnetic field equations can then be considered in the entire volume, and the solution of (2) is given by the Biot-Savart law

$$\vec{B}(\vec{r}) = \frac{\mu_0}{4\pi} \int_G \vec{J}(\vec{r'}) \times \frac{(\vec{r} - \vec{r'})}{|\vec{r} - \vec{r'}|^3} \, dv' \tag{7}$$

where $\vec{r}$ is the point of detection, $\vec{r'}$ is the coordinate of the primary and secondary dipoles, $\vec{J}(\vec{r'})$ is the current distribution in the conductor, and G is the volume of the region (Fig. 1).

Combining (4) and (7), we obtain

$$\begin{aligned} \vec{B}(\vec{r}) &= \frac{\mu_0}{4\pi} \int_G [\vec{J}_p - \sigma \nabla' \phi] \times \frac{(\vec{r} - \vec{r'})}{|\vec{r} - \vec{r'}|^3} \, dv' \\ &= \frac{\mu_0}{4\pi} \int_G \vec{J}_p \times \frac{(\vec{r} - \vec{r'})}{|\vec{r} - \vec{r'}|^3} \, dv' \\ &\quad - \frac{\mu_0}{4\pi} \int_G \sigma \nabla' \phi \times \frac{(\vec{r} - \vec{r'})}{|\vec{r} - \vec{r'}|^3} \, dv'. \end{aligned} \tag{8}$$

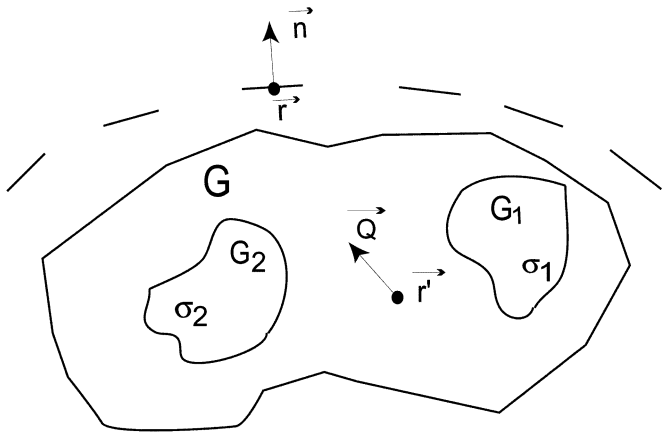

Fig. 1. Schematic diagram showing the relationship between $\vec{r}$ (coordinate point of detection), $\vec{n}$ (normal to the detector), $\vec{r'}$ (coordinate of the dipole), $\vec{Q}$ (moment of dipole), G (total conductive region), G_1 (conductive subregion 1), σ_1 (conductivity of subregion 1), G_2 (conductive subregion 2), σ_2 (conductivity of subregion 2). This example illustrates the use of variables for piecewise constant conductivity regions, but the equations are equally valid for continuously varying conductivities.

For a current dipole $\vec{J}_p(\vec{r}) = \vec{Q}\delta(\vec{r} - \vec{r_0})$ with moment $\vec{Q}$ and position $\vec{r_0}$

$$\vec{B}(\vec{r}) = \vec{B}_p(\vec{r}) - \frac{\mu_0}{4\pi} \int_G \frac{\sigma \nabla' \phi \times (\vec{r} - \vec{r'})}{|\vec{r} - \vec{r'}|^3} \, dv' \tag{9}$$

where

$$\vec{B}_p(\vec{r}) = \frac{\mu_0}{4\pi} \frac{\vec{Q} \times (\vec{r} - \vec{r_0})}{|\vec{r} - \vec{r_0}|^3}. \tag{10}$$

The integral portion of (9) models the magnetic field due to volume currents that are dependent upon the conductivity and electric potential, whereas the balance of the right hand side of (10) models the primary current which is independent of conductivity.

The detectors used in MEG measure only the normal component of the magnetic field [19]. Thus, (9) becomes

$$\vec{B}_n(\vec{r}) = \vec{B}_p(\vec{r}) \cdot \vec{n} - \frac{\mu_0}{4\pi} \int_G \sigma \nabla' \phi \times \frac{(\vec{r} - \vec{r'})}{|\vec{r} - \vec{r'}|^3} \, dv' \cdot \vec{n} \tag{11}$$

where $\vec{n}$ is the normal to the detector. These formulas, together with the Poisson equation, are used for the numerical computations in this paper.

Of note is that the gradient operator can be moved (see the Appendix) from the potential onto the conductivity term inside the integral

$$\vec{B}(\vec{r}) = \vec{B}_p(\vec{r}) + \frac{\mu_0}{4\pi} \int_G \frac{\phi \nabla' \sigma \times (\vec{r} - \vec{r'})}{|\vec{r} - \vec{r'}|^3} \, dv'. \tag{12}$$

Equation (12) shows that more significant contributions to the total magnetic field are expected in regions where σ changes the most, and that lesser gradients of σ should yield smaller contributions to the magnetic field due to volume currents. Thus, one would expect strong contributions to the total magnetic field

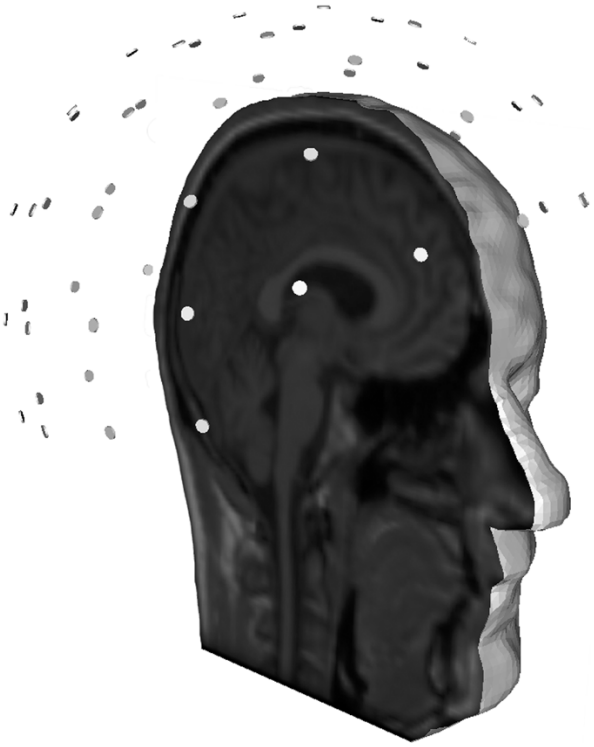

Fig. 2. Magnetic field detector positions in relation to one of the MRI slices used to form the FEM realistic head model.

from the skull/scalp boundary where a relatively large gradient of the conductivity is present.

III. Results

Our simulations employed a finite element method with linear basis functions to calculate the magnetic field in a model using realistic geometry [7], [20]. The model was constructed from a volume magnetic resonance image (MRI) scan of a 34 year old patient whose head had a radius of approximately 100 mm. The Biomedical Problem Solving Environment (BioPSE) [21] was used to solve the forward and inverse MEG simulations.

The realistic head model for the forward simulations consists of 72 745 nodes, 406 493 uniformally spaced tetrahedral elements, and 61 detectors placed over the head (Fig. 2). We considered six conductivity regions in the head and assigned them conductivity values from the literature: air ($\sigma = 0.0$ S/m), scalp ($\sigma = 1.0$ S/m), skull ($\sigma = 0.05$ S/m), CSF ($\sigma = 4.62$ S/m), gray matter ($\sigma = 1.0$ S/m), and white matter ($\sigma = 0.43$ S/m) [14]; these conductivity values were considered the baseline conductivities.

A. Realistic Head Forward Simulation

To determine the influence of head tissue conductivities on MEG forward calculations, we compared the normal component of the magnetic field at the MEG detectors of several realistic FEM head models, each model containing a different set of conductivity values for the head tissues, with results obtained using data generated from the same dipoles placed in the same locations in a realistic head model with the baseline set of head tissue conductivity values noted above. The conductivity values of the scalp, skull, CSF, gray matter, and white matter were varied, one at a time, to 10%, 25%, 50%, 75%, 110%, 125%, 150%, 175%, and 200% of the baseline value.

Eight current electric dipoles were individually placed into each of the altered conductivity models and the magnetic fields were calculated for each dipole individually. These dipoles were located in the gray matter of the left occipital cortex, the right occipital white matter, the right posterior frontal subcortical white matter, the white matter of the right anterior internal capsule, the gray matter of the anterior right cingulate gyrus, the left hippocampal white matter, the right medial temporal white matter, and the gray matter of the right globus pallidus. The dipole distance from the closest magnetic detector was 53.6, 53.8, 65.6, 84.5, 84.6, 92.5, 95.9, and 97.1 mm, respectively.

Equation (11) was used to calculate the normal component of the magnetic field at the detector points in the FEM models with the altered conductivity values and in the model with the baseline conductivity values. The ϕ in (11) implicitly depends upon σ and was obtained by solving the partial differential equations corresponding to the Poisson equation, (6). As can be seen in Table I, each of the five conductivity layers was altered to have each of the nine different conductivity values; only one layer and one conductivity value were changed in each model. The discrepancies between each model's results and those of the baseline model are reported in Table I as one minus the absolute value of the correlation coefficient expressed as a percent. For example, decreasing the scalp conductivity value to 75% of the baseline value resulted in a discrepancy between the normal component of the magnetic field at the detectors in the varied conductivity model and those in the baseline conductivity model of $0.754 \pm 0.158\%$; a decrease in the conductivity by 50% produced a difference of $6.36 \pm 12.2\%$.

B. Realistic Head Inverse Simulation

The normal component of the magnetic field was calculated at each detector by forward simulation for a single dipole in the baseline conductivity model. White Gaussian noise was added to the detectors' magnetic field data in a signal-to-noise ratio (SNR) of 9:1. The results of the forward simulation for this dipole, but not the dipole's location, were then used as the "measured" data with which to run an inverse MEG simulation using one of the head models with the altered tissue conductivity. In order to avoid biasing the solution in the source localization procedure, the realistic head model that was used in the forward simulation was modified to form a different mesh containing 72 749 nodes and 406 517 tetrahedral elements; this modified mesh was used in all inverse simulations realistic head model studies. The same 61 detector positions and orientations that were used in the forward model were employed to perform inverse simulations with the modified mesh model. The inverse simulation was performed by positioning a test dipole in one element of the altered conductivity finite element head mesh, finding the optimal magnitude and orientation for the dipole in that element using linear least squares optimization, and then computing the misfit between the forward solution for the test dipole and the "measured" data [22], [23]. The test dipole was then moved to different positions in the mesh until a position was found where the misfit between the forward solution for the test dipole and the "measured" data was minimized. Rather than

TABLE I
FORWARD MEG ERROR

Altered Tissue	Percentage of Baseline Conductivity Used in Model								
	10%	*25%*	*50%*	*75%*	*110%*	*125%*	*150%*	*175%*	*200%*
Scalp	39.9 ± 60.4%	24.1 ± 37.5%	6.36 ± 12.2%	0.754 ± 0.158%	0.217 ± 0.444%	0.401 ± 0.504%	1.30 ± 1.55%	2.56 ± 3.13%	4.17 ± 5.51%
Skull	2.20 ± 2.61%	1.06 ± 1.18%	0.313 ± 0.350%	$5.85\text{x}10^{-2}$ ± $6.60\text{x}10^{-2}$%	$6.84\text{x}10^{-3}$ ± $7.81\text{x}10^{-3}$%	$3.87\text{x}10^{-2}$ ± $4.33\text{x}10^{-2}$%	0.129 ± 0.149%	0.251 ± 0.290%	0.390 ± 0.453%
CSF	16.0 ± 34.3%	1.90 ± 2.82%	0.634 ± 0.940%	0.134 ± 0.212%	$1.89\text{x}10^{-2}$ ± $3.42\text{x}10^{-2}$%	0.115 ± 0.219%	0.445 ± 0.912%	0.976 ± 2.12%	1.69 ± 3.81%
Gray Matter	6.74 ± 10.3%	3.51 ± 5.41%	1.02 ± 1.40%	0.188 ± 0.217%	$2.34\text{x}10^{-2}$ ± $2.10\text{x}10^{-2}$%	0.137 ± 0.115%	0.513 ± 0.414%	1.12 ± 0.938%	1.97 ± 1.77%
White Matter	7.96 ± 7.74%	3.30 ± 2.38%	0.990 ± 0.711	0.205 ± 0.159%	$2.90\text{x}10^{-2}$ ± $2.68\text{x}10^{-2}$%	0.177 ± 0.180%	0.699 ± 0.829%	1.59 ± 2.16%	2.87 ± 4.37%

TABLE II
INVERSE MEG ERROR (MILLIMETERS)

Altered Tissue	Percentage of Baseline Conductivity Used in Model									
	10%	*25%*	*50%*	*75%*	*100%*	*110%*	*125%*	*150%*	*175%*	*200%*
Scalp	19.74 ± 18.35	9.82 ± 6.80	5.97 ± 4.09	3.10 ± 2.62	0.488 ± 0.806	3.35 ± 2.47	4.48 ± 4.03	5.72 ± 3.90	9.26 ± 5.56	10.62 ± 10.46
Skull	3.50 ± 2.67	1.73 ± 1.57	1.19 ± 0.72	1.34 ± 0.92	0.488 ± 0.806	2.30 ± 1.76	1.58 ± 1.38	2.61 ± 3.13	2.37 ± 2.02	3.12 ± 2.88
CSF	4.53 ± 5.88	3.49 ± 3.50	2.93 ± 2.60	2.28 ± 2.40	0.488 ± 0.806	1.60 ± 0.74	1.24 ± 1.11	1.78 ± 1.07	1.60 ± 1.32	1.42 ± 1.39
Gray Matter	4.33 ± 2.81	2.54 ± 1.75	2.27 ± 1.20	1.98 ± 1.27	0.488 ± 0.806	1.65 ± 1.47	1.86 ± 1.38	1.98 ± 2.16	2.17 ± 2.28	2.30 ± 2.52
White Matter	9.38 ± 6.96	8.23 ± 5.14	4.79 ± 3.14	4.19 ± 2.99	0.488 ± 0.806	3.10 ± 2.62	2.62 ± 1.77	3.43 ± 1.92	4.16 ± 2.83	5.58 ± 2.93

calculating the misfit for each element, the downhill simplex [2] optimization search technique was used starting at multiple points including the true dipole position which, if producing a bias at all, would tend to favor a more accurate localization of the dipole in the altered models.

Inverse MEG simulations were performed on data "measured" at detectors for the same eight dipole locations that were used in the forward study. The altered conductivity value models that were used in the inverse portion of the simulation contained conductivity values of the scalp, skull, CSF, gray matter, and white matter that were varied, one at a time, to 10%, 25%, 50%, 75%, 110%, 125%, 150%, 175%, and 200% of the baseline value. The inverse MEG solutions for each of the varied conductivity models were compared to the true dipole source position; localization errors are listed in Table II. For example, decreasing the scalp conductivity value to 75% of the baseline value resulted in a position error of 3.10 ± 2.62 mm, and a decrease by 50% produced an error of 5.97 ± 4.09 mm. Inverse simulations using the baseline conductivity values with the mesh and noise employed in all the inverse simulations resulted in an average error of 0.488 ± 0.806 mm.

As shown in Table II, changes in the scalp conductivity tended to cause greater localization errors than did the same percentage change in conductivity in other layers. The greater localization errors found for the changes in scalp conductivity differed significantly from the smaller errors found by changing the skull conductivity ($p < 0.025$, Multivariate Analysis of Variance followed by Scheffe's test), the CSF conductivity ($p < 0.041$), and the gray matter conductivity ($p < 0.037$), and tended to be greater than those found by changing the white matter conductivity ($p < 0.284$), especially for the larger changes in conductivity (e.g., 10% and 200%). Also, localization errors tended to be greater for changes in white matter conductivity than were found for changes in gray matter conductivity, although the differences in localization errors did not reach the level of statistical significance.

The dipoles used in the source localization study can be divided into two groups: dipoles that are >75 mm from the nearest detector (i.e., "deep" in the head), and dipoles that are <75 mm to a detector (i.e., in a more superficial location). When all models with varied conductivities are considered together, the position error for the "deep" dipoles tended to be greater than was the error for the superficial dipoles ($p < 0.08$, Multivariate Analysis of Variance); the lack of significance probably reflects the small sample size of the data. The error for "deep" dipoles also tended to be greater than the error for superficial dipoles for models in which the gray matter conductivity varied and for models in which the white matter varied. For example, for the "deep" dipoles, a decrease of the gray matter conductivity to 75% resulted in a position error of 2.45 ± 1.36 mm, and a decrease by 50% produced an error of 2.54 ± 1.48 mm. For the superficial dipoles, a decrease of the gray matter conductivity to 75% resulted in a position error of 1.52 ± 1.21 mm, and a decrease by 50% produced an error of 1.81 ± 0.38 mm. For the "deep" dipoles, a decrease of the white matter conductivity to 75% of the baseline value resulted in a position error of 5.47 ± 2.91 mm, and a decrease of 50% produced an error of 5.69 ± 3.48 mm. For the superficial dipoles, a decrease of the white matter conductivity to 75% resulted in a position error of 2.06 ± 1.88 mm, and a decrease by 50% produced an error of 3.30 ± 2.35 mm.

The same observations regarding "deep" versus superficial dipoles held for the scalp, skull, and CSF tissue layers, as well. The position error for the "deep" dipoles tended to be greater than the error for the superficial dipoles for the models in which the scalp conductivity varied, for the models in which the skull conductivity varied, and for the models in which the CSF conductivity varied.

The direction of the source localization error that resulted from models with varied conductivity values was investigated as well. When considering dipoles that were "deep", models with varied conductivities tended to result in source localization positions which were superficial to the true dipole position 74.1% of the time, regardless of whether the conductivity value used was greater or less than the baseline conductivity value. When considering superficial dipoles, models with varied conductivities tended to result in source localization positions which were "deep" relative to the true dipole position 68.0% of the time, regardless of whether the conductivity value used was greater or less than the baseline conductivity value. The source localization position which resulted when using a model with varied conductivities was always on the same side of the head as the true dipole position; no dipole was located incorrectly to the contralateral hemisphere. A dipole depth from 53 mm to 65 mm from the nearest detector appears to be the "cross-over" point between dipoles that tended to result in source localization errors that were more "deep" than the true dipole position and those that were more superficial than the dipole position.

C. Multiple Tissue Conductivity Changes

To test the effect of changing the conductivity values of more than one tissue layer simultaneously on the calculated magnetic field and source localization, three models were constructed for both forward and inverse simulations. In the first model, both the scalp and skull conductivities were altered. The second model contained altered gray and white matter conductivities. In the third model, conductivity values of all five layers were altered simultaneously. The same eight dipoles as were used in the Sections III-A and III-B were used in each of these models. For the inverse simulations, the realistic head model mesh used in Section III-B was used and white Gaussian noise was added to the forward simulated data in a SNR of 9:1 to represent the "measured" data.

Table III shows the forward and inverse errors of the results calculated from the models with altered tissue conductivities. The first column of Table III indicates the tissue layers that were altered and the amount that their conductivity values were changed as a percentage of the baseline conductivity values; the tissue layers and conductivities not shown for a particular model were left at the baseline conductivity values. The normal component of the magnetic field calculated at a detector using the model with the varied conductivity value was compared to the results obtained using the data generated using the baseline model and is shown in the second column of Table III as one minus the absolute value of the correlation coefficient expressed as a percent. The inverse MEG simulation was performed using a realistic head model with altered conductivities and the data "measured" from the forward simulation using the baseline conductivity model. The source localization for each of the varied conductivity models was compared to the true dipole source position; the errors for each model are listed in the third column of Table III.

TABLE III
MULTIPLE CONDUCTIVITY CHANGES: MEG FORWARD AND INVERSE ERRORS

Altered Tissues with Percentage of Baseline Conductivity Used in Model	Forward Error	Inverse Error
Scalp 90%, Skull 90%	0.166 ± 0.253%	2.35 ± 0.84mm
Scalp 110%, Skull 125%	0.207 ± 0.255%	3.38 ± 3.12mm
Scalp 110%, Skull 150%	0.377 ± 0.453%	3.97 ± 4.42mm
Scalp 75%, Skull 75%	1.43 ± 2.53%	3.44 ± 3.62mm
Scalp 125%, Skull175%	0.204 ± 0.286%	3.18 ± 2.54mm
Scalp 125%, Skull 125%	0.665 ± 0.793%	4.25 ± 4.32mm
Scalp 50%, Skull 50%	9.33 ± 18.4%	5.97 ± 3.72mm
Scalp 150%, Skull 50%	0.560 ± 0.718%	4.72 ± 3.77mm
Gray 90%, White 90%	$6.59\text{x}10^{-2}$ ± $6.50\text{x}10^{-2}$%	2.53 ± 2.20mm
Gray 110%, White 125%	0.226 ± 0.274%	2.56 ± 1.71mm
Gray 110%, White 150%	0.776 ± 1.01%	3.68 ± 1.93mm
Gray 75%, White 75%	0.449 ± 0.428%	4.95 ± 5.10mm
Gray 125%, White 75%	0.302 ± 0.280%	3.03 ± 3.34mm
Gray 125%, White 125%	0.382 ± 0.478%	1.25 ± 1.77mm
Gray 50%, White 50%	2.40 ± 2.81%	6.43 ± 5.56mm
Gray 150%, White 50%	1.88 ± 2.29%	5.47 ± 2.83mm
Scalp 110%, Skull 110%, CSF 110%, Gray 110%, White 110%	0.531 ± 0.646%	2.05 ± 2.30mm
Scalp 125%, Skul1 125%, CSF 75%, Gray 75%, White 75%	3.75 ± 4.96%	9.59 ± 6.63mm
Scalp 75%, Skull 75%, CSF 110%, Gray 110%, White 110%	2.71 ± 5.07%	4.71 ± 3.80mm
Scalp 110%, Skull 110%, CSF 75%, Gray 75%, White 75%	1.99 ± 2.43 %	6.42 ± 4.42mm

Table III illustrates representative examples of multiple conductivity changes, but is not exhaustive. When one considers all models in which the two tissue layers of the scalp and skull or gray and white matter conductivity values were changed simultaneously, increasing or decreasing both of the conductivities tended to result in larger forward and inverse errors than were found by decreasing one of the conductivity values and increasing the other conductivity value, but this trend did not reach the level of statistical significance.

Another example of multiple tissue conductivity values being altered simultaneously comes from the models used by other authors. Table IV contains the forward and source localization errors calculated for seven realistic head models containing conductivity values which have been used by other authors. When an author did not report a conductivity value for a particular tissue layer, the baseline conductivity value for that layer was used in the realistic head model. The same eight dipoles as were used in Sections III-A and III-B were used to calculate both the average forward and inverse errors. Each row is labeled by the tissues and their conductivity values in that model. The normal component of the magnetic field calculated at a detector using the model with the varied conductivity value was compared to the data from the baseline model and shown in Table IV as one minus the absolute value of the correlation coefficient expressed as a percent. The inverse MEG simulation was performed using the realistic head model with the altered conductivities, the realistic head mesh described in Section III-B, and the data "measured" from the forward simulation using the baseline conductivity model with added white Gaussian noise in a SNR of 9:1. The source localization for each of the varied con-

TABLE IV
OTHER FREQUENTLY USED CONDUCTIVITY VALUES: MEG FORWARD AND INVERSE ERRORS

Altered Tissues With Conductivity Values (S/m)	Forward Error	Inverse Error	Author Reference
Scalp 0.46, Skull 0.0058, CSF 1.39,Gray0.46, White 0.46	8.64 ± 1.48%	8.22 ± 4.61mm	Cohen, et al., 1983
Scalp1.0, Skull 0.0144, CSF 4.62, Gray 0.17,White 0.12	5.97 ± 9.13%	10.64 ± 11.27mm	Foster, et al., 1989
Scalp 1.0, Skull 0.025, CSF 3.00, Gray1.5, White 1.0	7.64 ± 12.9%	6.78 ± 4.45mm	Peters, et al., 1991
Scalp 0.43, Skull 0.00625, CSF 1.54, Gray 0.333, White 0.143	0.216 ± 0.149%	2.48 ± 2.35mm	Haueisen, 1996
Scalp 1.0, Skull 0.0125, CSF 1.0, Gray 1.0, White 1.0	7.21 ± 13.1%	7.64 ± 4.21mm	van den Broek,1997
Scalp 0.33, Skull 0.0042, CSF 0.33, Gray 0.33, White 0.33	7.14 ± 11.1%	7.15 ± 4.06mm	Huiskamp, et al., 1999
Scalp 1.0, Skull 0.05, CSF 1.25, Gray 0.285, White 0.256	16.8 ± 29.7%	13.94 ± 11.53mm	Latikka, et al., 2001

ductivity models was compared to the true dipole source position; errors are reported in Table IV. The reference for the conductivity values used in a particular model is given in the far right hand column of Table IV.

IV. DISCUSSION

Changing conductivity values of individual tissue layers did not result in random variations in forward and inverse solutions, but rather distinct trends in the solution errors were observed. Tables I and II show that for all five tissue layers, greater amounts of change from the baseline conductivity value for a single layer increases the error for both the forward and inverse computations. Equation (12) explains this observation. A large change in the conductivity from its baseline value in a tissue layer will result in a greater change in the gradient of σ across tissue barriers than will a small change in the conductivity of the same tissue. The greater the gradient, the larger would be the expected impact on the magnetic field; further, the greater the change in gradient, the larger would be the expected discrepancy from the baseline magnetic field.

Models with changes in the scalp conductivity value generally had larger errors in the predicted magnetic field values and in source localization than were found in models with a change in any other tissue layer, although Tables I and II show some variability exists. Equation (12) helps to explain this finding. The magnetic field due to the primary current is independent of the conductivity of the tissue layers and will give the same MEG value for a particular dipole and detector, regardless of the conductivity of the layers. In contrast, the magnetic field due to the volume currents varies as a function of the change in the conductivity at a barrier between two tissues. The magnetic field due to the volume currents is more influenced by the scalp conductivity than it is by any other layer for three reasons: 1) the large gradient between the conductivity of the scalp and the near zero conductivity of the air external to the head, 2) the large gradient between the skull and scalp conductivities, and 3) the scalp is the closest tissue layer to the detectors, thus $|\vec{r} - \vec{r'}|^3$ in (12) is at a minimum, and the influence of the scalp volume currents and conductivity on the total magnetic field are at a maximum.

The source localization errors calculated in models with changes in the conductivity value of some tissues often did not exceed the accuracy of MEG ($\sim$5 mm) [4]. Table II shows that small changes in the conductivity values of the skull or CSF, individually, do not impact the source localization error enough to be detected by MEG.

The magnetic field values calculated from models with changes in the white matter conductivity tended to have greater discrepancies than were found in those calculated from models with changes in the gray matter conductivity, although errors can occur with changes in the conductivity value for either gray or white matter. Similarly in source localization problems, changes in the white matter's conductivity value generally resulted in a larger localization error than did changes in the gray matter's conductivity value. The volume of the white matter in the brain is much larger than the volume of the gray matter. The integral portion of (11) applies to the entire volume of the brain, and conductivity value changes in the larger white matter volume would be expected to have a greater affect on the total magnetic field than would changes in the smaller volume of gray matter.

However, the larger volume of white matter does not totally explain the increased error in localization with changes in white matter conductivity. Often, the conductivity of the area directly surrounding the dipole has a greater influence on the resulting magnetic field than does the area further away from the dipole. As has been previously noted in a preliminary report of this study [24] and confirmed in two independent reports by Acar, *et al.* [25] and Miranda, *et al.* [26], the magnetic field resulting from dipoles located in the gray matter generally is more influenced by a change in gray matter conductivity than by a change in white matter conductivity, and the source localization error for such dipoles generally is larger when the gray matter conductivity value is changed than when the white matter conductivity value is changed. Conversely, the magnetic field resulting from dipoles located in the white matter generally is more influenced by a change in white matter conductivity than by a change in gray matter conductivity, and the source localization error for these dipoles generally is larger when the white matter conductivity value is changed than when the gray matter conductivity value is changed. The greater influence of the dipole's local environment would be expected from the integral portion of (11) that calculates volume currents. As the distance between the dipole and volume element decreases, $((\vec{r} - \vec{r'})/|\vec{r} - \vec{r'}|^3)$ increases and, thus, the influence of the local region's volume currents and conductivity on the total magnetic field increases.

For changes in the conductivity value in any tissue layer, the error associated with localizing "deep" dipoles tended to be greater than was the error associated with localizing dipoles more superficially located in the brain. Overall, the error in localizing "deep" dipoles tended to exceed the error for localizing superficial dipoles, although not statistically significant due to

small sample size ($p < 0.08$). Also, the error in localization of "deep" dipoles tended to be larger than was the error for localizing superficial dipoles for individual changes in conductivity values in the scalp, skull, CSF, gray matter, or white matter. The smaller localization errors found with superficial dipoles would be expected based on (11); for superficially located dipoles, the magnetic field due to the primary current dominates over the relatively low contributions from the magnetic field due to volume currents, and hence conductivity has little influence on the total measured magnetic field.

When tissue conductivity values were changed simultaneously, substantially larger errors often could occur in both the predicted magnetic fields and in the source localization of the dipoles than when the values were changed individually, as shown in Table III. This result is expected since multiple sources of error in the model would likely increase the inaccuracy of the calculated magnetic field. Although most of the source localization errors that occurred when the conductivity value of the different tissue layers was individually changed by 25% or 50% were less than the accuracy of MEG, the errors that occurred when more than one layer was varied were often greater than MEG's accuracy and could become of practical significance. A change of conductivity value of 25% or 50% may seem large, but the difference between the largest and smallest reported conductivity values of normal gray and white matter vary by as much as 200% and 50%, respectively [14], [11], [9], [12], [15]. Large differences in tissue conductivity values not only have been reported by different investigaors but by the same investigator in difference subjects; recent results by Goncalves, *et al.* [27] experimentally support the variability of the brain and skull conductivity values by reporting that the conductivity of the brain/skull ratio varies considerably from subject to subject with a mean ratio of 72 but a standard deviation of 48%. Also, if the brain is treated as a homogeneous volume conductor, then the conductivity of the gray and/or white matter may again vary up to 200% and 50%, respectively, of their reported individual conductivities. As noted above, the magnetic field appears to have a particular sensitivity to scalp conductivity; depending on the oils and perspiration that are present on the scalp, the conductivity value of the scalp may vary greatly. Further, conductivity changes that may occur in pathologic states are largely unknown, but could be expected to even exceed 200% in some circumstances, such as porencephalic cysts in gray or white matter.

The forward and source localization errors that occurred when all of the tissue layers were simultaneously altered could result in either substantial or trivial errors depending upon the ratio of the conductivity value alterations that took place. Although a change in the conductivity value by 50% was necessary before the error would be detectable by MEG when two tissue layers were varied at the same time, simultaneous changes in the scalp, skull, CSF, gray and white matter conductivity values could produce source localization errors that were greater than the accuracy of MEG for even a 10% or 25% change in the tissue layer's conductivity values, such as when the scalp and skull were given 110% of their baseline value and the CSF, gray and white matter were given 75% of their baseline value.

Table IV demonstrates the variability in the conductivity values that have been reported in the literature for head tissues. Using the conductivity values reported by other investigators instead of the baseline values used in this study led to MEG source localization errors sometimes greater than 1 cm, such as in the cases of Latika, *et al.* [12] and Foster, *et al.* [9]. We do not wish to imply that the baseline conductivity values that we have used are correct or that the tissue conductivity values used by other authors are incorrect. Rather, we only wish to point out that given the variation in reported conductivity values, a large localization error may occur when inaccurate tissue conductivity values are used for a particular patient or when one investigator's reported values are substituted into another's model. Accurate measurements and subsequent model representation of tissue conductivities would appear to be essential for accurate source localization in the human brain.

V. Conclusion

Conductivity values of the head tissues do influence the magnetic field resulting from a dipolar source in the brain. The conductivity of the tissue directly surrounding a dipole influences the resulting magnetic field more than does tissue that is farther away, and "deep" dipoles generally are more influenced by changed conductivity values than are dipoles that are more superficially located. Scalp conductivities also appear to influence the detected magnetic field more than do the conductivities of most other tissues. Although an alteration in a single tissue's conductivity value results in a small localization error, changes in conductivity in multiple tissues may have substantial affects on dipole source localization. Although a 50% change in conductivity may seem large, different investigators have published conductivity values for head tissue that can vary by this amount or more, and changes of this size may occur in pathologic states. This study suggests that accurate scalp, skull, CSF, gray and white matter conductivities may be important for MEG source localization in human brain.

VI. Future Work

In the future, we plan to continue to investigate the importance of using realistic finite element head models for forward and inverse MEG simulations. We plan to perform a study similar to the one presented, but on the effect of conductivity for distributed source models. We also plan to study quantitatively the effect of anisotropy within the head on normal components of the magnetic field as measured by MEG, and how these anisotropies influence both forward and inverse MEG simulations.

Appendix
Proof for (12)

We start with (9) from Section II

$$\vec{B}(\vec{r}) = \vec{B}_p(\vec{r}) - \frac{\mu_o}{4\pi}\int_V \frac{(\sigma\nabla'\phi)\times(\vec{r}-\vec{r'})}{\|\vec{r}-\vec{r'}\|^3}\,dv'. \qquad (13)$$

In order to evaluate the integral, we first use differentiation by parts

$$\sigma(\nabla\phi) = \nabla(\sigma\phi) - (\nabla\sigma)\phi. \tag{14}$$

Substituting this expression back into (13), we have

$$\vec{B}(\vec{r}) = \vec{B}_p(\vec{r}) - \frac{\mu_o}{4\pi}\int_V \frac{\nabla'(\sigma\phi)\times(\vec{r}-\vec{r'})}{\|\vec{r}-\vec{r'}\|^3}\,dv' + \frac{\mu_o}{4\pi}\int_V \frac{(\nabla'\sigma)\phi\times(\vec{r}-\vec{r'})}{\|\vec{r}-\vec{r'}\|^3}\,dv'. \tag{15}$$

We are interested in evaluating the second integral in the above expression. Introducing $\vec{R} = \vec{r} - \vec{r'}$ and using $\nabla(1/R) = -\vec{R}/R^3$, the second integrand in (15) can be written

$$\begin{aligned}&\frac{\nabla'(\sigma\phi)\times(\vec{r}-\vec{r'})}{\|\vec{r}-\vec{r'}\|^3}\\ &= \nabla'(\sigma\phi)\times\frac{(\vec{r}-\vec{r'})}{\|\vec{r}-\vec{r'}\|^3} = \nabla'(\sigma\phi)\times\frac{\vec{R}}{R^3}\\ &= -\nabla'(\sigma\phi)\times\nabla'(1/R).\end{aligned} \tag{16}$$

A useful vector identity can be obtained for the *curl* of a scalar-vector product

$$\nabla\times(f\vec{b}) = f(\nabla\times\vec{b}) + (\nabla f)\times\vec{b}. \tag{17}$$

If we choose $\vec{b} = \nabla g$ then

$$\nabla\times(f(\nabla g)) = f(\nabla\times(\nabla g)) + (\nabla f)\times(\nabla g) \tag{18}$$

but the first term on the right hand side of this expression is the curl of the gradient which is always zero. Thus, (18) can be simplified to

$$\nabla\times(f(\nabla g)) = (\nabla f)\times(\nabla g). \tag{19}$$

Comparing (16) and (19) we can write

$$\nabla'(\sigma\phi)\times\nabla'(1/R) = \nabla'\times((\sigma\phi)\nabla'(1/R)). \tag{20}$$

Finally, we use the Stoke's theorem that links volume and surface integrals

$$\int_V \nabla\times\vec{F}\,dv = \int_S d\vec{S}\times\vec{F}. \tag{21}$$

The second term from (15) then becomes

$$\begin{aligned}&\int_V \frac{\nabla'(\sigma\phi)\times(\vec{r}-\vec{r'})}{\|\vec{r}-\vec{r'}\|^3}\,dv'\\ &= -\int_V \nabla'(\sigma\phi)\times\nabla'(1/R)\,dv'\\ &= -\int_V \nabla'\times((\sigma\phi)\nabla'(1/R))\,dv'\\ &= -\int_S d\vec{S'}\times((\sigma\phi)\nabla'(1/R)).\end{aligned} \tag{22}$$

The surface integral in this expression is evaluated on the surface surrounding the entire volume and its value should be computed as $r' \to \infty$. Then

$$\left\|\int_S d\vec{S'}\times((\sigma\phi)\nabla'(1/R))\right\| \sim \sigma(r)\phi(r)(1/r^2)r^2 \sim \sigma(r)\phi(r). \tag{23}$$

Since $\phi(r=\infty) = 0$ from the Poisson equation solution and $\sigma(r=\infty) = 0$ due to the problem's geometry, the integral is in fact zero.

Finally, the gradient operator can be moved from the potential onto the conductivity term inside the integral

$$\vec{B}(\vec{r}) = \vec{B}_p(\vec{r}) + \frac{\mu_o}{4\pi}\int_V \frac{\phi\nabla'\sigma\times(\vec{r}-\vec{r'})}{\|\vec{r}-\vec{r'}\|^3}\,dv'. \tag{24}$$

ACKNOWLEDGMENT

The authors would like to thank B. Davis of the Center for High Performance Computing at the University of Utah, and Lajos Horvath and B. Young of the Mathematics Department at the University of Utah for their assistance with the statistics, D. Weinstein of the SCI Institute for his helpful comments on the paper, and N. Galli of the SCI Institute for his assistance in generating the figures. The BioPSE software that was used for this research is available from our NIH NCRR center website: www.sci.utah.edu/ncrr.

REFERENCES

[1] J. Mosher, R. Leahy, and P. Lewis, "Matrix Kernels for the Forward Problem in EEG and MEG," Los Alamos National Labs, Tech. Rep. LA-UR-97-3812, 1997.

[2] ——, "EEG and MEG: Forward solutions for inverse methods," *IEEE Trans. Biomed. Eng.*, vol. 46, pp. 245–259, Mar. 1999.

[3] R. Gulranjani, *Bioelectricity and Biomagnetism*. New York: Wiley, 1998.

[4] M. Hämäläinen, R. Hari, R. Ilmoniemi, J. Knuutila, and O. Lounasmaa, "Magnetoencephalography—Theory, instrumentation, and applications to noninvasive studies of the working human brain," *Rev. Modern Phys.*, vol. 65, pp. 413–497, 1993.

[5] J. Sarvas, "Basic mathematical and electromagnetic concepts of the biomagnetic inverse problem," *Phys. Med. Biol.*, vol. 32, pp. 11–22, 1987.

[6] R. Van Uitert and C. Johnson, "Can a spherical model substitute for a realistic head model in forward and inverse MEG simulations?," in *Proc. 13th Int. Conf. Biomagnetism*, 2002, pp. 798–800.

[7] R. Van Uitert, D. Weinstein, and C. Johnson, "Volume currents in forward and inverse magnetoencephalographic simulations using realistic head models," *Ann. Biomed. Eng.*, vol. 31, pp. 21–31, 2003.

[8] D. Cohen and B. N. Cuffin, "Demonstration of useful differences between magnetoencephalogram and electroencephalogram," *Electroencphalogr. Clin. Neurophysiol.*, vol. 56, pp. 38–51, 1983.

[9] K. Foster and H. Schwan, "Dielectric properties of tissues and biological materials: A critical review," *Crit. Rev. Biomed. Eng.*, vol. 17, pp. 25–104, 1989.

[10] J. Haueisen, C. Ramon, M. Eiselt, H. Brauer, and H. Nowak, "Influence of tissue resistivities on neuromagnetic fields and electric potentials studied with a finite element model of the head," *IEEE Trans. Biomed. Eng.*, vol. 44, pp. 727–735, Aug. 1997.

[11] G. Huiskamp, J. Maintz, G. Wieneke, M. Viergever, and A. van Huffelen, "The influence of the use of realistic head geometry in the dipole localization of interictal spike activity in MTLE patients," in *Proc. 1st Int. Symp. Noninvasive Functional Source Imaging Within the Human Heart and Brain*, 1997, pp. 84–87.

[12] J. Latikka, T. Kuurne, and H. Eskola, "Conductivity of living intracranial tissue," *Phys. Med. Biol.*, vol. 46, pp. 1611–1616, 2001.
[13] T. Oostendorp, J. Delbeke, and D. Stegeman, "The conductivity of the human skull: Results of *in vivo* and *in vitro* measurements," *IEEE Trans. Biomed. Eng.*, vol. 47, pp. 1487–1492, Nov. 2000.
[14] M. Peters and J. D. Munck, "The influence of model parameters on the inverse solution based on MEG's and EEGs," *Acta Otolaryngol*, vol. 491, pp. 61–69, 1991.
[15] B. van den Broek, "Volume conduction effects in EEG and MEG," Ph.D. Dissertation, Univ. Twente, Twente, The Netherlands, 1997.
[16] D. Burnett, *Finite Element Analysis: From Concepts to Applications*. Reading, MA: Addison-Wesley, 1987.
[17] J. Jin, *The Finite Element Method in Electromagnetics*. New York: Wiley, 1993.
[18] R. Van Uitert, D. Weinstein, C. Johnson, and L. Zhukov, "Finite element EEG and MEG simulations for realistic head models: Quadratic vs. linear approximations," in *Proc. 3rd Int. Symp. Noninvasive Functional Source Imaging Within the Human Heart and Brain*, 2001, pp. 32–34.
[19] J. Malmivuo and R. Plonsey, *Bioelectromagnetism*. Oxford, U.K.: Oxford Univ., 1995.
[20] D. Weinstein and C. Johnson, "Effects of geometric uncertainty on the inverse EEG problem," in *Computational, Experimental, and Numerical Methods for Solving Ill-Posed Inverse Imaging Problems: Medical and Nonmedical Applications*, R. Barbour, M. Carvlin, and M. Fiddy, Eds: SPIE (Int. Soc. Opt. Eng.), 1997, vol. 3171, pp. 138–145.
[21] BioPSE: Biomedical Problem Solving Environment. Software. NIH Center for Bioelectric Field Modeling, Simulation, and Visualization. [Online]. Available: www.sci.utah.edu/ncrr
[22] D. Weinstein, L. Zhukov, and C. Johnson, "Lead-field bases for electroencephalography source imaging," *Ann. Biomed. Eng.*, vol. 28, pp. 1–7, 2000.
[23] L. Zhukov, D. Weinstein, and C. Johnson, "Independent component analysis for EEG source localization," *IEEE Eng. Med. Biol. Mag.*, vol. 19, pp. 87–96, May-June 2000.
[24] R. Van Uitert and C. Johnson, "Influence of brain conductivity on magnetoencephalographic simulations in realistic head models," in *Proc. 25th Annu. Int. Conf. IEEE Engineering in Medicine and Biology Society*, vol. 3, 2003, pp. 2136–2139.
[25] C. E. Acar and N. Gençer, "Sensitivity of EEG and MEG to conductivity perturbations," in *Proc. 25th Annu. Int. Conf. IEEE Engineering in Medicine and Biology Society*, vol. 3, 2003, pp. 2834–2837.
[26] P. C. Miranda, M. Hallett, and P. J. Basser, "The electric field induced in the brain by magnetic simulation: A 3-D finite-element analysis of the effect of tissue heterogeneity and anisotropy," *IEEE Trans. Biomed. Eng.*, vol. 50, pp. 1074–1085, Sept. 2003.
[27] S. Goncalves, J. de Munck, J. Verbunt, R. Heethaar, and F. da Silva, "*In vivo* measurement of brain and skull resistivities using an EIT-based method and the combined analysis of SEF/SEP data," *IEEE Trans. Biomed. Eng.*, vol. 50, pp. 1124–1128, Sept. 2003.

Robert Van Uitert (S'04) received the B.S. degree in computer science from Stanford University, Stanford, CA, in 1998. He is currently working towards the Ph.D. degree in computer science at the Scientific Computing and Imaging Institute at the University of Utah, Salt Lake City.

His research interests are in the field of scientific computing. His particular interests include inverse problems, biomedical computing, scientific visualization, and imaging problems.

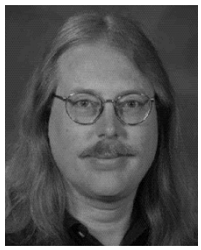

Chris Johnson (M'95–A'95–SM'04) directs the Scientific Computing and Imaging Institute at the University of Utah, Salt Lake City, where he is a Distinguished Professor of Computer Science and holds faculty appointments in the Departments of Physics, and Bioengineering. His research interests are in the area of scientific computing. His particular interests include inverse and imaging problems, adaptive methods, problem solving environments, biomedical computing, and scientific visualization. He founded the SCI research group in 1992 which has since grown to become the SCI Institute employing over 70 faculty, staff, and students. He serves on several international journal editorial boards, as well as on advisory boards to several national research centers.

Leonid Zhukov received the B.S and M.S. degrees in physics from Moscow Engineering and Physics Institute, Moscow, Russia, in 1991 and 1993, and the Ph.D. degree from University of Utah, Salt Lake City, in 1998.

He is currently a Senior Research Scientist at Yahoo! Research Labs. and Visiting Faculty member at the Department of Computer Science at the California Institute of Technology, Pasadena. His research interests are in the field of scientific computing, simulation, and visualization. His specific interests include inverse problems, multiresolution methods, large-scale computational problems, and dimensionality reduction techniques.